Title

Polymorphism in M(H$_2$PO$_2$)$_3$ (M = V, Al, Ga) compounds with the perovskite-related ReO$_3$ structure

Journal

Chemical Communications, 55(20)

ISSN

1359-7345 1364-548X

Authors

Evans, Hayden A
Deng, Zeyu
Collings, Ines E
et al.

Publication Date

2019

DOI

10.1039/c9cc00118b

Peer reviewed

Journal Name

ARTICLE TYPE

Cite this: DOI: 10.1039/xxxxxxxxxx

Polymorphism in $M(H_2PO_2)_3$ (M = V, Al, Ga) compounds with the perovskite-related ReO_3 structure.

Hayden A. Evans,[ab‡] Zeyu Deng,[cd‡] Ines E. Collings,[e] Yue Wu,[c] Jessica L. Andrews,[a] Kartik Pilar,[b], Joshua M. Tuffnell,[f] Guang Wu,[a] John Wang,[c] Siân E. Dutton,[f] Paul D. Bristowe,[d] Ram Seshadri,[abg] and Anthony K. Cheetham,[bcd]

Received Date
Accepted Date

DOI: 10.1039/xxxxxxxxxx

www.rsc.org/journalname

Trivalent metal hypophosphites with the general formula $M(H_2PO_2)_3$ (M = V, Al, Ga) adopt the ReO_3 structure, with each compound displaying two structural polymorphs. High-pressure synchrotron X-ray studies reveal a pressure-driven phase transition in $Ga(H_2PO_2)_3$ that can be understood on the basis of *ab initio* thermodynamics.

The AMX_3 perovskite structure — well known for accommodating a wide range of chemical substitution — has engendered many interesting compounds and countless avenues of material research. The versatility of the perovskite structure arises from the flexibility to substitute on any of the three chemical sites, A, M, or X, with the tolerance factor serving as a proxy for stability.[1,2] Over the past decade, there has been considerable focus on hybrid (organic-inorganic) halide perovskites which show great promise in optoelectronic technologies,[3–6] as well as the related class of alkylammonium metal(II) formates $(A)Mn^{II}(HCO_2)_3$[7] which can display ferroelectric and multiferroic behaviour.[8,9] Hypophosphite perovskites $AM(H_2PO_2)_3$ compounds are also known.[10,11]

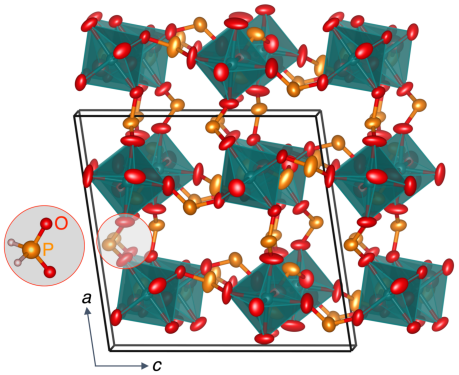

Fig. 1 Representative crystal structure with the ReO_3 topology of α-$M(H_2PO_2)_3$, shown for M = Ga in the $P2_1/n$ space group (90 % ellipsoids, H removed for clarity). The inset displays the complete hypophosphite $H_2PO_2^-$ anion.

While not as numerous, there have also been parallel discoveries of ReO_3-type materials. These compounds are A site deficient: $\square MX_3$, where $\square$ is a vacancy. MX_3 compounds can vary in X site composition, very much in the manner of AMX_3 perovskites. Besides the oxide (ReO_3),[12] this class includes fluorides,[13] nitrides,[14] and examples with molecular anions.[15,16] Some recently reported molecular-anion containing compounds include $Ln(BH_4)_3$,[17] $Ln[C(NH)_2(NH)]_3$,[18] In(imidazolate)$_3$[19], and the $M[Bi(SCN)_6]$ series,[20] demonstrating the impressive richness of X site composition of MX_3 compounds. Since ReO_3 structure materials are known for interesting conductive,[17,21] structural,[22,23] barocaloric,[24] and optical properties,[20,25] the ability to control composition is promising from the materials design viewpoint.

In a recent report on the new family of $AMn^{2+}(H_2PO_2)_3$ perovskites made by some of us,[10] it was noted that only one ReO_3-type $M(H_2PO_2)_3$ compound, $V^{3+}(H_2PO_2)_3$, has been documented to date.[26] We refer to this compound as α-$V(H_2PO_2)_3$ and employ Greek letters throughout this work to denote unique ReO_3-

‡ *These authors contributed equally to this work.*
[a]*Department of Chemistry and Biochemistry, University of California Santa Barbara, California 93106 United States.*
[b]*Materials Research Laboratory, University of California Santa Barbara, California 93106 United States. E-mail: akc30@cam.ac.uk*
[c]*Department of Materials Science and Engineering, National University of Singapore Singapore 117575, Singapore*
[d]*Department of Materials Science and Metallurgy, University of Cambridge 27 Charles Babbage Rd, CB3 0FS Cambridge, UK*
[e]*European Synchrotron Radiation Facility 71 avenue des Martyrs, 38000 Grenoble, France*
[f]*Cavendish Laboratory, Department of Physics, University of Cambridge JJ Thomson Avenue, Cambridge CB3 0HE, United Kingdom*
[g]*Materials Department, University of California Santa Barbara, California 93106 United States*
† Electronic Supplementary Information (ESI) available. This includes experimental details, crystallographic files (CCDC 1888648 – 1888652), PXRD, NMR, TGA, and additional DFT calculations. See DOI: 10.1039/b000000x/

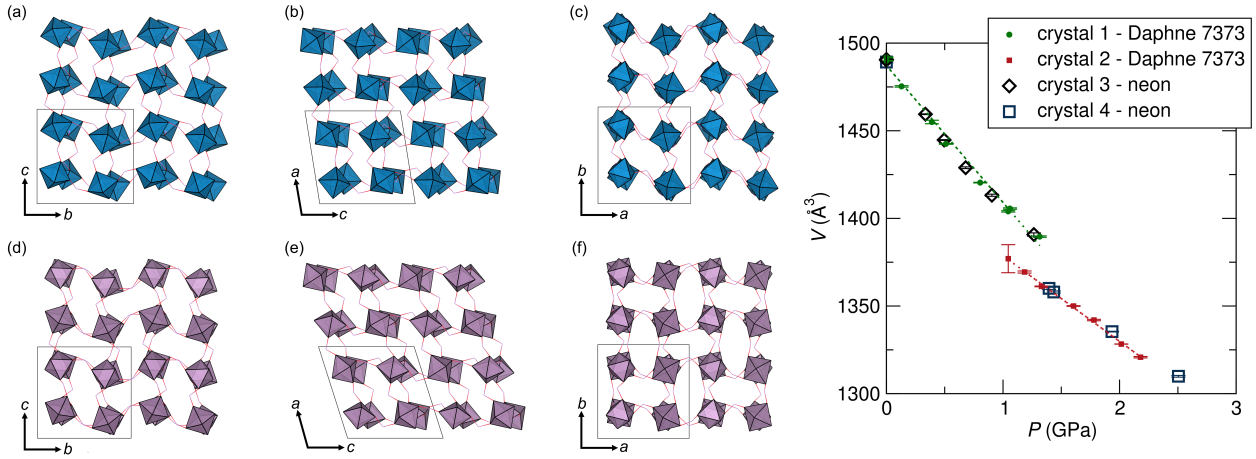

Fig. 2 Pressure-induced phase transition of α-Ga$(H_2PO_2)_3$. (a,b,c) Views of the ambient pressure crystal structure ($P2_1/n$, β=98.55°) along the a, b, and c axes. (d,e,f) Views of the high pressure crystal structure ($P2_1/n$, β=107.68°) along the a, b, and c axes. The graph depicts the cell volumes as a function of pressure of four crystals tested using two different pressure transmitting mediums; Daphne 7373 oil and neon gas. The volume drop upon the phase transition can be observed between ≈1.2 GPa and 1.40 GPa. Each crystal was examined over certain ranges to mitigate radiation damage. The ranges for the Daphne oil crystals were 0 GPa – 1.3 GPa, and 1.0 GPa to 2.2GPa, and for the neon crystals 0 GPa – 1.3 GPa, and 0, 1.4 GPa – 4.8 GPa. The Daphne 7373 oil crystal data was fit with a second order Birch-Murnaghan equation of state (dashed lines).

type polymorphs. In the initial report of α-V$(H_2PO_2)_3$, the connection with ReO_3 was not noted, and the structure was simply described as 3D connected, with each V atom octahedrally coordinated with $H_2PO_2^-$ anions. Inspired by the general interest in ReO_3 type materials, we believed that other related compounds could be made. We report here the successful preparation of a new family of $M(H_2PO_2)_3$ compounds, where M = V, Al, and Ga, (representative structure displayed in Figure 1), and describe the intriguing polymorphism that each member displays. We also study one of the compounds, α-Ga$(H_2PO_2)_3$, as a function of hydrostatic pressure, finding a hysteretic first-order phase transition close to a pressure of 1 GPa. We complement the structural work with detailed density functional theory (DFT)-based thermodynamic examination of the P–T phase diagrams of the three systems.

In the original study of α-V$(H_2PO_2)_3$, crystals of α-V$(H_2PO_2)_3$ were isolated from a solvothermal reaction between V_2O_3, H_3PO_2, and $Li_2(CO_3)$, and the structure was solved using single crystal X-ray diffraction (SCXRD).[26] Based on powder X-ray diffraction (PXRD) of the bulk product, α-V$(H_2PO_2)_3$ was then established as a minor product alongside an undetermined major phase. Per our subsequent modification of the reported procedure, we successfully isolated crystals of a second polymorph, β-V$(H_2PO_2)_3$, and Rietveld analysis of the bulk product suggests that this is the unidentified major phase.† The β phase ($P2_1/c$) is distinct from the α phase ($P2_1/n$), presenting a less distorted ReO_3 framework. Unlike single atom anion perovskites (*e.g.* oxides), which display predictable in-phase or out-of-phase octahedral tilt and rotation patterns, molecular anions induce octahedral tilts, rotations, and shifts that are quite complex owing to the greater degrees of freedom. As such, expanded Glazer notation can be used to better describe these systems, and this analysis is presented in the ESI for the phases described in this work.†[11,27,28]

For the remaining $M(H_2PO_2)_3$ family members, the metals Al and Ga were chosen as likely M site candidates because of their preferred 3+ oxidation states and similar ionic radii to V^{3+}: 0.640 Å, 0.535 Å, and 0.620 Å, respectively for octahedral V^{3+}, Al^{3+}, and Ga^{3+}. It was found that the Al system has two preferred phases: α-Al$(H_2PO_2)_3$, and a new γ-Al$(H_2PO_2)_3$ phase. Both polymorphs are obtained together using a solvothermal reaction between H_3PO_2 and Al(O-i-Pr)$_3$, producing α-Al$(H_2PO_2)_3$ as approximately 10% of the final product, per Rietveld analysis.† Although we were unable to make phase-pure α-Al$(H_2PO_2)_3$, we successfully prepared phase pure γ-Al$(H_2PO_2)_3$ by substituting γ-Al_2O_3 for Al(O-i-Pr)$_3$ in the solvothermal reaction. The γ phase polymorph crystallizes in the space group $C2/c$ and like the β phase, presents a less distorted structure when compared to the α phase. Interestingly, we have found that while the structure of Al$(H_2PO_2)_3$ has not been reported, this composition has generated a substantial amount of interest as a flame retardant. When aluminum hypophosphite is added to a polymer blend, there is evidence that the anion reduces the mass transfer pathway, increasing thermal stability,[29] in addition to, in some cases, altering the degradation mechanism.[30]

In all of the synthesis attempts, the Ga system only yielded α-Ga$(H_2PO_2)_3$ with high phase purity crystal quality. Consequently, high pressure SCXRD experiments were carried out at the European Synchrotron Radiation Facility (ESRF). We hypothesized that under pressure α-Ga$(H_2PO_2)_3$ may transform to one of the aforementioned, less distorted and consequently denser, polymorphs (β or γ phases). Figure 2 displays views of the structure of α-Ga$(H_2PO_2)_3$ below and above its pressure-induced phase transition, as well as a plot of T *vs.* P from the SCXRD refinements at each pressure. As is quite evident, α-Ga$(H_2PO_2)_3$ undergoes a first-order phase transition near 1.0 GPa to another phase, which is neither β or γ. Instead, α-Ga$(H_2PO_2)_3$ undergoes a classical isomorphic phase transition to a phase with the same connectiv-

Table 1 Polymorphs seen in all members of the $M(H_2PO_2)_3$ family. The columns of each polymorph indicate if/how that phase presents in each metal system. The largest possible pore diameter (Å) is included in parenthesis.

	α ($P2_1/n$)	β ($P2_1/c$)	γ ($C2/c$)	δ ($P2_1/n$)
V	minor (1.05)	major (0.87)	–	–
Al	minor (0.96)	–	major (0.61)	–
Ga	sole (0.95)	–	–	high pressure (0.71)

ity and space group $P2_1/n$, but with an increased crystallographic β angle of 107.68° (instead of 98.55°). We refer to this high-pressure phase as the δ phase. Upon releasing of this pressure, the α phase is recovered. The bulk modulus of the α phase obtained from the X-ray data is 14.3 GPa, which is substantially lower than the corresponding value for the denser, high pressure δ-phase (27.0 GPa).† This is typical behavior for open-to-dense phase transitions under pressure.

In total, we have observed four polymorphs between all M variants studied, with each metal system displaying two polymorphs. Table 1 summarizes these polymorphs, and specifies whether they are the minor, major, sole, or high pressure phases. Crystallographic details of each polymorph can be found in the ESI.† It should be noted that the α phase is a shared polymorph between all metal systems at ambient temperature and pressure. However, each system shows distinct behavior, with the Ga system found solely as the α phase under ambient conditions, whereas for Al and V, the α phase occurs only as a minor phase. Considering what would appear to be subtle differences between the α, β, γ, and δ phases, it is curious that certain polymorphs are seen in some metal systems, and not in others. We shed light on this question through DFT calculations by comparing the stability within each systems of the two preferred polymorphs as P and T are varied. The free energy as a function of P and T was calculated by combining DFT and lattice dynamics calculations, as described previously for perovskite formates.[31] Figure 3 displays the results from the free energy calculations for the three metal systems, with the results further discussed below. We also provide additional details of the thermodynamic analysis in the ESI.†

Figure 3(a) shows the stability of the two observed polymorphs for the V system (α and β) as T and P are varied. It can be seen that at ambient temperature and pressure, that the β phase is the preferred polymorph, which is consistent with what is observed experimentally. We had great difficulty synthetically isolating the α phase in our experiments following the reported procedure, and based on Rietveld analysis, it appeared that the only phase observed was the β phase. However, to grow suitable crystals of either phase, we found that the inclusion of Li_2CO_3 was essential (as in the previous report), which could also explain how the α phase may form as a metastable product. Figure 3(b) shows the stability of the two observed polymorphs for the Al system (α and γ). From these calculations our observation of more than one Al polymorph is not surprising, as the calculations suggest that both

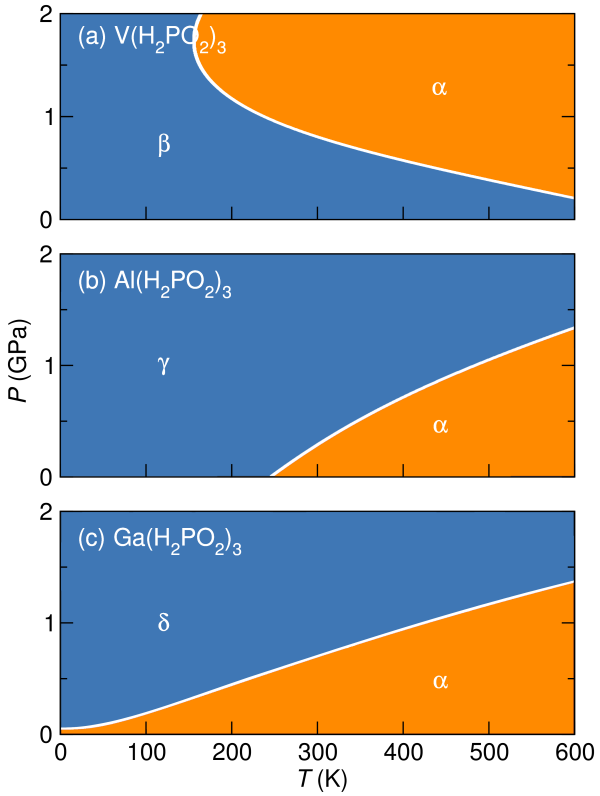

Fig. 3 Calculated P–T phase diagrams for each metal system, and the two observed polymorphs seen each in each. (a) V system, α–β polymorphs. (b) Al system, α–γ polymorphs. (c) Ga system, α–δ polymorphs.

polymorphs are expected to be stable at around ambient T and P. However, due to our success with isolating the γ phase pure by using γ-Al_2O_3, it is feasible that there may well be a synthetic strategy to isolating the α phase pure if the right conditions can be met. Figure 3(c) shows the stability of the two observed polymorphs for the Ga system (α and δ). These calculations predict that the α phase is the preferred phase at ambient pressure and all temperatures, and the δ phase will only form under pressure. This was confirmed experimentally via low temperature PXRD experiments, where no phase transition was observed between 300 K and 12 K.† The stability of the α phase down to very low temperatures arises due to its lower zero-point energy relative to the δ phase (Table S8).†

It is interesting to note that the α phase is not only common to all three systems, but is also the high temperature phase in each case. The calculations illustrate this by indicating that the α phases have higher entropies compared to the low temperature/high pressure phases.† One can regard the high temperature and low temperature phases as open and closed pore systems, respectively, in a manner that is qualitatively similar to certain metal-organic frameworks, such as ZIF-4[32] and MIL-53.[33] In particular, larger pores are well known to give rise to enhanced vibrational entropies. The greater pore radii in the α-phases are tabulated in Table 1. The magnitudes of the free volume effects are much smaller than those that have been seen in the metal-organic frameworks (MOFs), but the thermodynamic consequences are

similar.

An issue around the formation of the $M(H_2PO_2)_3$ polymorphs is the potential for additional effects due to hydrogen bonding. Surprisingly, there appears to be weak P–H$\cdots$O hydrogen bonding in the α phase, across the faces of the open cavities. In the more dense polymorphs, like the γ-$Al(H_2PO_2)_3$ or the high pressure δ-$Ga(H_2PO_2)_3$ phase, hydrogen bonding does not appear to be present on inspection of the P–H$\cdots$O distances. This is an interesting effect and appears analogous to other perovskite-related systems which display void space due to the effects of hydrogen bonding forces.[34] Finally, it is informative to compare this ReO_3-type hyphophosphite family with a closely related family of formate MX_3 compounds. Although the hyphosphites are made absent of any observable moiety within the cavities, the formate family is only isolable when made in the presence of CO_2, which then resides within the cavities and stabilizes the material.[35] For the hypophosphite system this is not the case, as the pore size (diameter of less than 2 Å) is too small as a consequence of the extra H atoms. This was further confirmed in pressure experiments with neon as a pressure-transmitting medium, where no neon (atomic diameter of 2.4 Å)[36] was found to enter the cavities of the $Ga(H_2PO_2)_3$ structure.

In conclusion, we present a new family of $M(H_2PO_2)_3$ compounds displaying unusual polymorphism. Based on the size of the metal cation, certain polymorphs are favored at ambient pressure and temperature, with one phase being shared throughout. Entropic stabilization appears to play an important role in stabilizing the structures.

Conflicts of interest

There are no conflicts to declare.

Acknowledgments

This work was supported by the U.S. Department of Energy, Office of Science, Basic Energy Sciences under award number DE-SC-0012541. The use of the Shared Experimental Facilities of the Materials Research Science and Engineering Center (MRSEC) at UCSB is gratefully acknowledged (NSF DMR 1720256). We acknowledge the provision of beamtime at the European Synchrotron Radiation Facility on the ID15B beamline for the high-pressure work. IEC thanks J. Jacobs for the neon gas load. Calculations were performed using the Cambridge HPCS and the UK National Supercomputing Service, ARCHER. Access to the latter was obtained via the UKCP consortium and funded by EPSRC under Grant No. EP/P022596/1. AKC thanks the Ras al Khaimah Centre for Advanced Materials for financial support.

Notes and references

1 V. M. Goldschmidt, *Naturwissenschaften*, 1926, **14**, 477–485.
2 G. Kieslich, S. Sun and A. K. Cheetham, *Chem. Sci.*, 2014, **5**, 4712–4715.
3 A. Kojima, K. Teshima, Y. Shirai and T. Miyasaka, *J. Am. Chem. Soc.*, 2009, **131**, 6050–6051.
4 C. C. Stoumpos and M. G. Kanatzidis, *Acc. Chem. Res.*, 2015, 150909082443006.
5 D. H. Fabini, J. G. Labram, A. J. Lehner, J. S. Bechtel, H. A. Evans, A. Van der Ven, F. Wudl, M. L. Chabinyc and R. Seshadri, *Inorg. Chem.*, 2016, **56**, 11–25.
6 B. Saparov and D. B. Mitzi, *Chem. Rev.*, 2016, **116**, 4558–4596.
7 X.-Y. Wang, L. Gan, S.-W. Zhang and S. Gao, *Inorg. Chem.*, 2004, **43**, 4615–4625.
8 P. Jain, N. S. Dalal, B. H. Toby, H. W. Kroto and A. K. Cheetham, *J. Am. Chem. Soc.*, 2008, **130**, 10450–10451.
9 P. Jain, V. Ramachandran, R. J. Clark, H. D. Zhou, B. H. Toby, N. S. Dalal, H. W. Kroto and A. K. Cheetham, *J. Am. Chem. Soc.*, 2009, **131**, 13625–13627.
10 Y. Wu, S. Shaker, F. Brivio, R. Murugavel, P. D. Bristowe and A. K. Cheetham, *J. Am. Chem. Soc.*, 2017, **139**, 16999–17002.
11 Y. Wu, T. Binford, J. A. Hill, S. Shaker, J. Wang and A. K. Cheetham, *Chemical Commun.*, 2018, **54**, 3751–3754.
12 D. V. S. Muthu, P. Teredesai, S. Saha, U. V. Waghmare, A. K. Sood and C. N. R. Rao, *Phys. Rev. B*, 2015, **91**, 224308.
13 B. K. Greve, K. L. Martin, P. L. Lee, P. J. Chupas, K. W. Chapman and A. P. Wilkinson, *J. Am. Chem. Soc.*, 2010, **132**, 15496–15498.
14 R. K. Sithole, L. F. E. Machogo, M. A. Airo, S. S. Gqoba, M. J. Moloto, P. Shumbula, J. Van Wyk and N. Moloto, *New J. Chem.*, 2018, **42**, 3042–3049.
15 A. A. Karyakin, *Electroanalysis*, 2001, **13**, 813–819.
16 S. Ferlay, T. Mallah, R. Ouahes, P. Veillet and M. Verdaguer, *Nature*, 1995, **378**, 701.
17 M. B. Ley, M. Jørgensen, R. Cerny, Y. Filinchuk and T. R. Jensen, *Inorg. Chem.*, 2016, **55**, 9748–9756.
18 A. L. Goörne, J. George, J. van Leusen, G. Dück, P. Jacobs, N. K. Chogondahalli Muniraju and R. Dronskowski, *Inorg. Chem.*, 2016, **55**, 6161–6168.
19 M. E. Schweinefuß, I. A. Baburin, C. A. Schröder, C. Näther, S. Leoni and M. Wiebcke, *Cryst. Growth Des.*, 2014, **14**, 4664–4673.
20 M. J. Cliffe, E. N. Keyzer, M. T. Dunstan, S. Ahmad, M. F. L. De Volder, F. Deschler, A. J. Morris and C. P. Grey, *Chem. Sci.*, 2019, **42**, 3042–3049.
21 A. Ferretti, D. B. Rogers and J. B. Goodenough, *J. Phys. Chem. Solids*, 1965, **26**, 2007–2011.
22 J. O. Ticknor, B. R. Hester, J. W. Adkins, W. Xu, A. A. Yakovenko and A. P. Wilkinson, *Chem. Mater.*, 2018, **30**, 3071–3077.
23 C. Yang, P. Tong, J. C. Lin, X. G. Guo, K. Zhang, M. Wang, Y. Wu, S. Lin, P. C. Huang and W. Xu, *Appl. Phys. Lett.*, 2016, **109**, 23110.
24 A. Corrales-Salazar, R. T. Brierley, P. B. Littlewood and G. G. Guzmán-Verri, *Phys. Rev. Mater.*, 2017, **1**, 53601.
25 C. G. Granqvist, *Appl. Phys. A*, 1993, **57**, 3–12.
26 H. A. Maouel, V. Alonzo, T. Roisnel, H. Rebbah and E. Le Fur, *Acta Crystallogr. C*, 2009, **65**, i36–i38.
27 J. A. Hill, A. L. Thompson and A. L. Goodwin, *J. Am. Chem. Soc.*, 2016, **138**, 5886–5896.
28 H. L. B. Boström, J. A. Hill and A. L. Goodwin, *Phys. Chem. Chem. Phys*, 2016, **18**, 31881–31894.
29 W. Yang, Z. Jia, Y. Chen, Y. Zhang, J. Si, H. Lu and B. Yang, *RSC Adv.*, 2015, **5**, 105869–105879.
30 B. Zhao, L. Chen, J.-W. Long, H.-B. Chen and Y.-Z. Wang, *Ind. Eng. Chem. Res.*, 2013, **52**, 2875–2886.
31 G. Kieslich, S. Kumagai, K. T. Butler, T. Okamura, C. H. Hendon, S. Sun, M. Yamashita, A. Walsh and A. K. Cheetham, *Chem. Commun.*, 2015, **51**, 15538–15541.
32 M. T. Wharmby, S. Henke, T. D. Bennett, S. R. Bajpe, I. Schwedler, S. P. Thompson, F. Gozzo, P. Simoncic, C. Mellot-Draznieks, H. Tao, Y. Yue and A. K. Cheetham, *Angew. Chem. Int. Ed.*, 2015, **54**, 6447–6451.
33 A. Boutin, F.-X. Coudert, M.-A. Springuel-Huet, A. V. Neimark, G. Férey and A. H. Fuchs, *J. Phys. Chem. C*, 2010, **114**, 22237–22244.
34 H. A. Evans, D. H. Fabini, J. L. Andrews, M. Koerner, M. B. Preefer, G. Wu, F. Wudl, A. K. Cheetham and R. Seshadri, *Inorg. Chem.*, 2018, **57**, 10375–10382.
35 Y.-Q. Tian, Y.-M. Zhao, H.-J. Xu and C.-Y. Chi, *Inorg. Chem.*, 2007, **46**, 1612–1616.
36 J. K. Badenhoop and F. Weinhold, *J. Chem. Phys.*, 1997, **107**, 5422–5432.

Supporting Information:

Polymorphism in $M(H_2PO_2)_3$ (M = V, Al, Ga) compounds with the perovskite-related ReO_3 structure.

E-mail:

Hayden A. Evans,[ab‡] Zeyu Deng,[cd‡] Ines E. Collings,[e] Yue Wu,[c] Jessica L. Andrews,[a] Kartik Pilar,[b], Joshua M. Tuffnell,[f] Guang Wu,[a] John Wang,[c] Siân E. Dutton,[f] Paul D. Bristowe,[d] Ram Seshadri,[abg] and Anthony K. Cheetham,[bcd]

‡ *These authors contributed equally to this work.* [a]*Department of Chemistry and Biochemistry, University of California, Santa Barbara, California 93106 United States.* [b]*Materials Research Laboratory, University of California, Santa Barbara, California 93106 United States* [c]*Department of Materials Science and Engineering, National University of Singapore, Singapore 117575, Singapore* [d]*Department of Materials Science and Metallurgy, University of Cambridge, 27 Charles Babbage Rd, CB3 0FS Cambridge, UK* [e]*European Synchrotron Radiation Facility, 71 avenue des Martyrs, 38000 Grenoble, France* [f]*Cavendish Laboratory, Department of Physics, University of Cambridge, JJ Thomson Avenue, Cambridge CB3 0HE, United Kingdom* [g]*Materials Department, University of California, Santa Barbara, California 93106 United States*

Experimental Information

Bulk β-$V(H_2PO_2)_3$ was prepared with a modified procedure from Maouel *et al.*[1] 0.100 g (0.550 mmol) V_2O_5 (Strem 98%), and 1.426 g (10.8 mmol) H_3PO_2 aqueous solution (Spectrum, 50% wt/wt) were combined in a teflon lined Parr vessel and heated from room temperature to 150°C over the course of 24 hours (≈0.1°C/min), held at 150°C for 48 hours, and then cooled from 150°C to room temperature over the course of 24 hours (≈0.1°C/min). A solid green *puck* of β-$V(H_2PO_2)_3$ was isolated from a green mother liquor via vacuum filtration. This puck was broken up, washed with copious amounts of H_2O then ethanol, and lastly vacuum dried at 60°C overnight. For small crystals of β-$V(H_2PO_2)_3$, the same procedure can be followed with the addition of 0.180 g (2.43 mmol) Li_2CO_3 (Sigma-Aldrich, 99.0%) to the V_2O_5 and H_3PO_2 solution. This should be allowed to off-gas CO_2 before sealing the Parr vessel.

A sample of $Al(H_2PO_2)_3$, that contained both α- and γ-$Al(H_2PO_2)_3$, was prepared as follows: 0.124 g (0.61 mmol) $Al(O\text{-}i\text{-}Pr)_3$ and 1.426 g (10.8 mmol) H_3PO_2 aqueous solution (Spectrum, 50% wt/wt) were combined in a teflon lined Parr vessel and placed into a preheated oven at 150°C oven for 24 hours. This Parr vessel was then removed from the oven, and air cooled to room temperature. The white colored product was then isolated from a clear/grey mother liquor via vacuum filtration, washed with copious amounts of H_2O then ethanol, and vacuum dried at 60°C overnight. We observed no difference in product composition if a longer heating profile, like that used for β-$V(H_2PO_2)_3$, was implemented. The final white colored product had larger cube-habit crystals that could be separated with visual assistance from an optical microscope. These larger cube-habit crystals were α-$Al(H_2PO_2)_3$, with the remainder of the white powder being small crystals of γ-$Al(H_2PO_2)_3$. A pure γ $Al(H_2PO_2)_3$ sample was prepared by using 0.055 g (0.53 mmol) γ-Al_2O_3 (Strem, 97%) instead of $Al(O\text{-}i\text{-}Pr)_3$ following the same procedure. Corundum Al_2O_3 cannot be used instead of γ-Al_2O_3, as corundum Al_2O_3 will not react under these conditions. For small crystals of γ-$Al(H_2PO_2)_3$, the procedure using γ-Al_2O_3 can be followed,

with the addition of 0.180 g (2.43 mmol) Li_2CO_3 (Sigma-Aldrich, 99.0%) to the γ-Al_2O_3 and H_3PO_2 solution. This mixture should be allowed to off-gas CO_2 before sealing the Parr vessel.

A phase pure sample of α-$Ga(H_2PO_2)_3$ was prepared by combining 0.09 g (0.48 mmol) Ga_2O_3 and 1.426 g (10.8 mmol) H_3PO_2 aqueous solution (Spectrum, 50% wt/wt) in a teflon lined Parr vessel, heating for 24 hours in a preheated 150°C oven, and removed to air cool. This product, which produced 1 mm$\times$1 mm$\times$1 mm clear crystals of α-$Ga(H_2PO_2)_3$, was washed with H_2O then ethanol, and vacuum dried at 60°C overnight.

Single crystal X-ray diffraction data was collected on a Bruker KAPPA APEX II diffractometer equipped with an APEX II CCD detector using a TRIUMPH monochromator with a Mo Kα X-ray source (λ = 0.71073 Å). The crystals were mounted on a cryoloop under Paratone-N oil. Absorption correction of the data was carried out using the multi-scan method as implemented in SADABS.[2] Subsequent calculations were carried out using SHELXTL.[3] Structure determination was done using intrinsic methods. Structure solution, refinement, and creation of publication data was performed using SHELXTL. Crystal structures were visualized using the VESTA software suite.[4]

High-pressure SCXRD data were measured for $Ga(H_2PO_3)_2$ at the ID15B beamline of the European Synchrotron Radiation Facility, Grenoble up to 2.2 GPa with Daphne 7373 oil as the pressure-transmitting medium (PTM) and up to 4.8 GPa with neon as the PTM at room temperature, using monochromatic X-ray radiation (λ = 0.41112).[5] Membrane driven LeToullec type diamond anvil cells (DACs) were used, equipped with Boehler-Almax anvils. Stainless steel was used as the gasket material, Daphne 7373 oil was loaded as the PTM, as it is non-penetrating and non-reactive,[6] while neon was used in the second loading to try and induce neon entry into the framework pores upon compression. Diffraction patterns were collected with a Mar555 flat panel detector. For the single-crystal data collection, steps of 0.5° oscillation were used over a total ω-scan range of 76° about the vertical axis. The single crystals were centred on the rotation axis using their absorption

profile from the X-rays. Lattice parameter determination and integration of the reflection intensities were performed using the *CrysAlisPro* software suite.[7] Two different crystals were loaded in the gasket chamber in order to increase the chances of solving potential high-pressure phases. The single crystal structures were refined using shelxL, and structure solution was performed with shelxT, within shelXle.[8–10] The pressures were measured using the ruby fluorescence method before and after each diffraction measurement. The reversibility of the phase transition was checked by measuring single-crystal data upon decompression.

Void space calculations were performed with the Mercury Software suite. A grid spacing of 0.1 Å was used for all calculations as probe radius was varied.[11]

Room temperature powder X-ray diffraction was performed on a Panalytical Empyrean Powder Diffractometer (Bragg-Brentano HD module, no monochromator) equipped with a Cu source $\lambda = 1.5418$ Å. Rietveld refinements were performed in the TOPAS software suite.[12] Variable temperature measurements $T = 12$–300 K were collected on a Bruker D8 Advance diffractometer, using an Oxford Cryosystems PheniX stage from $2\theta = 5°$–$120°$ with step size of $2\theta = 0.0204°$ and Cu Kα sources, $\lambda = 1.54$ Å.

Thermogravimetric analysis (TGA) on all compounds was conducted using a TA Instruments Discovery instrument. A rate of 25 cm^3/min dry nitrogen purge was employed with a temperature ramp rate of 10°C/min. The maximum temperature of the experiment was 900°C.

NMR experiments were done using a Bruker Avance 800 MHz NMR spectrometer with a solid-state 2.5 mm HX double resonance magic angle spinning (MAS) probe. $Ga(H_2PO_2)_3$ was packed in a zirconia rotor and spun at 35 kHz. Single pulse experiments (SPE) were carried out for ^{1}H and ^{31}P nuclei with resonant frequencies of 800 and 324 MHz, respectively. Additionally, a ^{31}P spectrum was obtained with ^{1}H decoupling to minimize ^{1}H-^{31}P dipole-dipole interactions to achieve narrower ^{31}P linewidths. An 8 μs and 1.9 μs 90° pulse was used to excite ^{1}H and ^{31}P nuclei, respectively, with an 80 s and 800 s recycle delay

between ^{1}H and ^{31}P scans. ^{31}P T_1 measurements were conducted using a saturation recovery pulse sequence. Relaxation curves were fit using Bruker Dynamics Center software and were found to be single component in nature. Density functional theory (DFT) calculations were performed using the projector augmented wave (PAW)[13,14] potential as implemented in VASP code[17,18] with following electrons treated explicitly: Al $3s^2 3p^1$, V $3s^2 3p^6 3d^3 4s^2$, Ga $4s^2 4p^1 3d^{10}$, P $3s^2 3p^3$, H $1s^1$, O $2s^2 2p^4$. A planewave kinetic energy cutoff of 500 eV and a Γ centered k-point Monkhorst Pack mesh[19] with a density of 0.25 Å^{-1} were chosen for all calculations. The PBE functional[20] was used and van der Waals forces were treated using the Tkatchenko-Scheffler scheme.[21] **Ga system**: The α phase and δ high pressure phase of the Ga system were fully relaxed (atomic coordinates and unit cell shape) starting from experimental results until interatomic forces were less than 0.01 eV/Å only with the constrain of their volume. Then the relaxed α phase and δ phase structures were further relaxed at different fixed volumes to obtain *E-V* relationship. These *E-V* values were used for the fitting of the Birch-Murnaghan equation of state:[22]

$$E(V) = E_0 + \frac{9V_0B_0}{16}\left\{\left[(\frac{V_0}{V})^{\frac{2}{3}}) - 1\right]^3 B_0' + \left[(\frac{V_0}{V})^{\frac{2}{3}} - 1\right]^2\left[6 - 4(\frac{V_0}{V})^{\frac{2}{3}}\right]\right\} \quad (1)$$

Following parameters were obtained from the fitting: equilibrium volume (V_0), equilibrium bulk modulus (B_0) and the derivative of the bulk modulus with respect to external pressure (B_0) as shown in Table S6. The external pressures in Figure S19 were calculated using the same equation of state in the pressure-volume expression:

$$P(V) = \frac{3B_0}{2}\left[(\frac{V_0}{V})^{7/3} - (\frac{V_0}{V})^{5/3}\right]\left\{1 + \frac{3}{4}(B_0' - 4)\left[\frac{V_0}{V}^{2/3} - 1\right]\right\} \quad (2)$$

Gibbs free energies of α and δ phases were calculated using the finite displacement method under the quasi-harmonic approximation (QHA) as implemented in the Phonopy code[23]

by minimizing the following term by changing volume:

$$G(P,T) = \underset{V}{min}\left[U(V) + F_{phonon}(T;V) + PV\right] \tag{3}$$

Due to the size of the unit cell $\approx$ 1400 Å^3 (128 ions), only the single unit cell was used for calculations to reduce the computational expenses. Before phonon calculations, structures were further relaxed using an 800 eV cutoff until the interatomic forces smaller than 0.001 eV/Å. A 10×10×10 Monkhorst Pack mesh[19] is used for phonon density of states sampling. Vibrational entropies at different pressures and temperatures were calculated using:[24]

$$S(P,T) = \int_0^T \frac{C_P(P,T')}{T'} dT' \tag{4}$$

, where C_P is the constant pressure heat capacity as given out by Phonopy. Pressure (volume) dependent bulk modulus were calculated using:

$$B = V\left(\frac{\partial^2 F}{\partial V^2}\right) \tag{5}$$

, where F is the Helmholtz free energy, and the external pressure can be obtained from volume using the equation of state above. The zero-point vibration energy (E_{ZP}) is evaluated by:

$$E_{ZP} = G - E_0 - PV \tag{6}$$

, where G is the Gibbs free energy and E_0 is the equilibrium ground state energy for equilibrium structure, PV term is 0 at ambient pressure.

DFT calculations for nuclear magnetic shift predictions were done using Vienna Ab initio Simulation Package (VASP).[17,18] The generalized gradient approximation (GGA) Perdew-Burke-Ernzerhof (PBE) was utilized for structural relaxations and NMR parameter calculations.[20] Structural relaxations were performed from initial conditions obtained via XRD data with rigid cell parameters. A Γ-centered $3\times3\times3$ k-mesh was used to sample the Brillouin zone. The plane-wave basis set cut-off energy was set to 600 eV during relaxation calculations and 800 eV for NMR parameter calculations. NMR chemical shielding tensors were calculated using gauge included projector augmented wave (GIPAW) formalism.[25]

Crystallographic information

All structures reported were solved via single crystal X-ray diffraction with relevant crystallographic data summarized in Tables S1 and S2. The CCDC deposition numbers are 1888648 – 1888652. One B alert was found for the reported β-V(H_2PO_2)$_3$ .cif related to the wR_2 value of 0.42; a result from the twinned crystal that was used for structure solution. B alerts were also found in the two α phase systems related to the close packed nature of the oxygens surrounding the metal atom.

Table S1: Crystallographic data β-$V(H_2PO_2)_3$, α-$Al(H_2PO_2)_3$, and γ-$Al(H_2PO_2)_3$.

Empirical Formula	$V(H_2PO_2)_3$ (β)	$Al(H_2PO_2)_3$ (α)	$Al(H_2PO_2)_3$ (γ)
Crystal habit, color	plate, green	cube, clear	plate, clear
Crystal system	monoclinic	monoclinic	monoclinic
Space group (#)	$P2_1/c$ (14)	$P2_1/n$ (14)	C_2/c (15)
Volume (Å^3)	764.7(1)	1454.9(2)	691.0(1)
T (K)	273	230	100
a (Å)	11.922(8)	11.2333(7)	11.95(1)
b (Å)	7.542(6)	11.5158(6)	7.809(8)
c (Å)	8.860(6)	11.3670(5)	7.868(9)
α (°)	90	90	90
β (°)	106.29(2)	98.320(4)	109.77(2)
γ (°)	90	90	90
Z	4	4	4
ρ (g mol^{-1})	245.90	443.88	221.94
Dens. (g cm^{-3})	2.136	2.026	2.133
Abs. (mm^{-1})	1.898	0.911	0.960
F_{000}	488	896	448
Reflections (unique)	1215(691)	9237 (2566)	2843 (552)
R_{int}	0.2330	0.1232	0.0934
R_1	0.1509	0.0554	0.0462
wR_R	0.3856	0.1017	0.0784
∂F (eÅ^{-3})	1.423 & −1.600	0.530 & −0.812	0.587 & −0.502
GOF	1.095	1.002	0.973

Table S2: Crystallographic data α-Ga(H_2PO_2)$_3$ and δ-Ga(H_2PO_2)$_3$.

Empirical Formula	Ga(H_2PO_2)$_3$ (α)	Ga(H_2PO_2)$_3$ (δ)
Crystal habit, color	cube, clear	cube, clear
Crystal system	monoclinic	monoclinic
Space group (#)	$P2_1/n$ (14)	$P2_1/n$ (14)
Volume (Å^3)	1489.4(4)	1361.2(3)
T (K)	296(2)	293(2)
P (GPa)	0	1.33
a (Å)	11.293(2)	11.3584(6)
b (Å)	11.614(2)	11.1052(1)
c (Å)	11.482(2)	11.327(2)
α (°)	90	90
β (°)	98.547(4)	107.68(1)
γ (°)	90	90
Z	4	4
ρ (g mol^{-1})	529.36	529.36
Dens. (g cm^{-3})	2.361	2.583
Abs. (mm^{-1})	4.312	1.044
F_{000}	1040	1040
Reflections (unique)	8720 (2801)	4568 (1925)
R_{int}	0.0961	0.0315
R_1	0.0464	0.0274
wR_R	0.0525	0.0697
∂F ($e\mathring{A}^{-3}$)	0.749 & -0.892	0.412 & -0.291
GOF	1.158	1.107

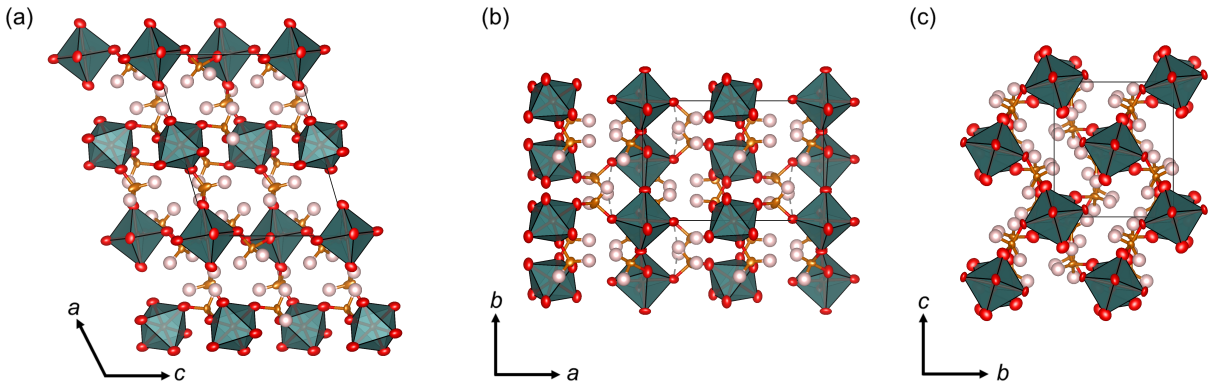

Figure S1: Views of β-V$(H_2PO_2)_3$ with 50% thermal elipsoids.

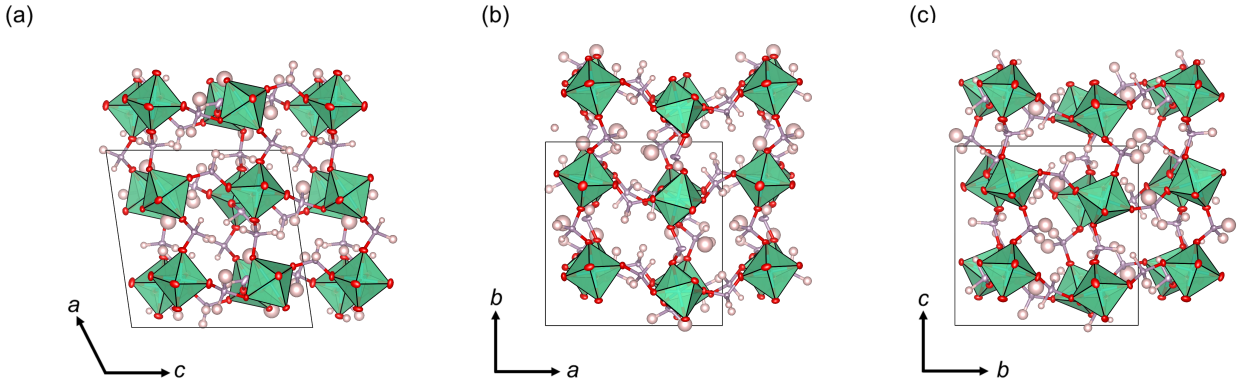

Figure S2: Views of α-Al$(H_2PO_2)_3$ with 50% thermal elipsoids.

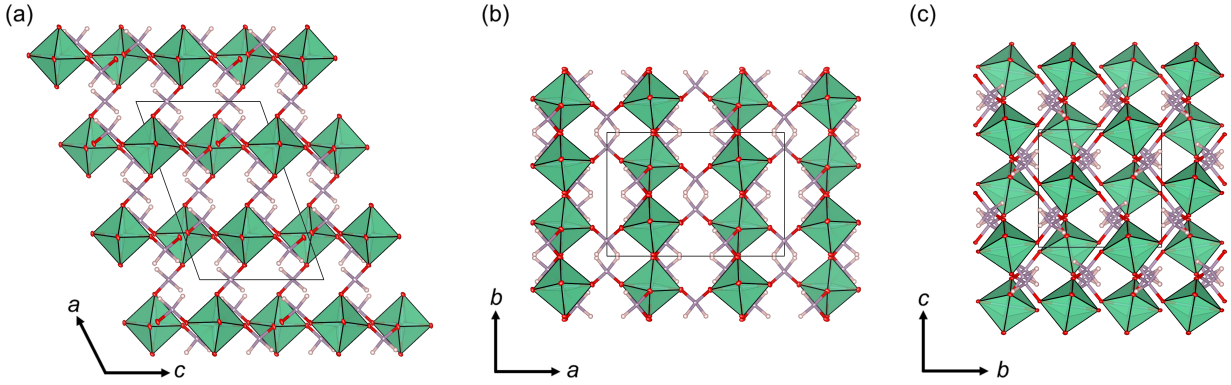

Figure S3: Views of γ-Al$(H_2PO_2)_3$ with 50% thermal elipsoids.

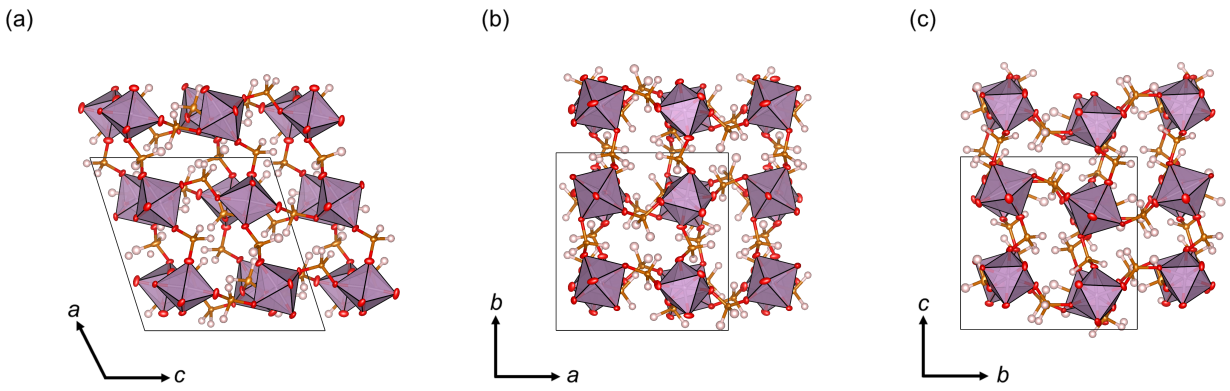

Figure S4: Views of δ-Ga$(H_2PO_2)_3$ with 50% thermal elipsoids.

Expanded Glazer notation

Octahedral tilting and columnar shifts of the reported phases are assigned as described by Boström and co-workers,[26] and used in our previous paper on hypophosphite-based dense frameworks.[27] The method for assigning these tilts and shifts are summarised in the latter paper: "[the matrix notation for octahedral tilting and columnar shifts] extend Glazer's widely used tilt notation to allow description of the additional correlation of distortions possible in perovskite analogues with polyatomic *X* ions. These are manifested as the rotation of octahedra (tilts) or the displacement of columns or planes of octahedra (shifts). Both tilt and shift descriptors each take the form of a 3×3 matrix. The diagonal terms in the tilt matrix can be determined by looking down the relevant pseudo-cubic axis and correspond to the normal Glazer terms. The off-diagonal terms are determined by taking slices of the structure For example, in the bc plane, the correlation of rotations around a propagating in b and c give the off-diagonal terms of the first row. In perovskites with monoatomic *X*, the off-diagonal terms are constrained to be '–' if tilts are active or '0' if they are inactive. The full tilt matrix is constructed from generalised Glazer terms $g_{ij} = \epsilon_i exp[2\pi i k_i j]$, with ϵ = (0,1) indicating whether a tilt is active, while k is the wavevector of the propagation. We draw attention to the periodicity of the tilt – most known perovskites, including hybrids, are either in phase $k = 0$, $g = 1$ ['+' by contention]) or out-of-phase

(k = 1/2, g = -1['$-$' by convention]). For the hypophosphite systems, we see values of $-0.5 + \sqrt{3}/2i$ (k =1/3), i (k =1/4), and $0.5 + \sqrt{3}/2i$ (k =1/6) – that is, periodicities of 3, 4 and even 6 octahedra. These periodicities do not uniquely describe patterns of rotation; for example, we see a variety of k = 1/4 tilts here. Shifts can likewise be assigned by considering slices of the structure. Each off-diagonal corresponds to the properties of a shift polarized along that axis. By convention, the diagonal terms are '+' if shifts are active in that axis or 0 if they are inactive; the remaining two terms correspond to the correlations in the two perpendicular directions."

In Figures S5–S8, we show views for each $M(H_2PO_2)_3$ phase down a pseudocubic axes a, b, and c, and describe the tilt and shift patterns in terms of these axes rather than the crystallographic ones. The crystallographic axes relative to each pseudocubic axes are denoted at the bottom left hand corners of each panel. The magnitude of octahedral tilting in these systems is much higher than in the $AM(H_2PO_2)_3$ perovskites. We believe this to be related to the greater degree of structural rigidity provided by the *A*-site cations. The most pronounced examples of increased octahedral tilting are seen in the β-V$(H_2PO_2)_3$ and γ-Al$(H_2PO_2)_3$ compounds.

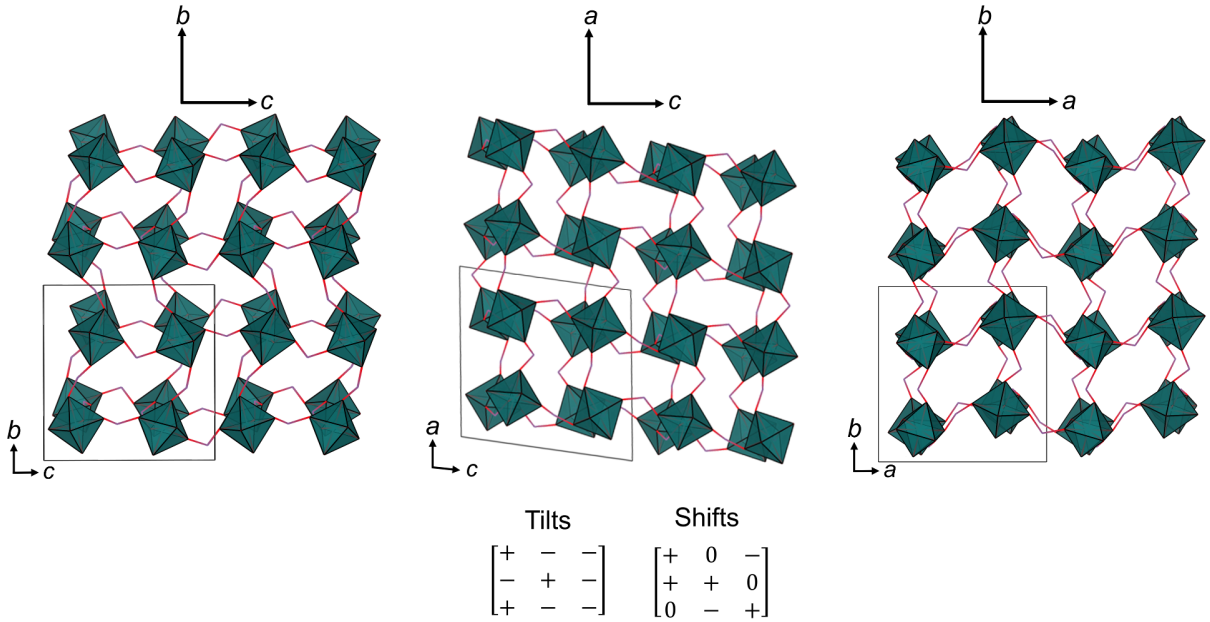

Figure S5: Views of the pseudocubic axes of α-$M(H_2PO_2)_3$ (M = V, Al, Ga. $P2_1/n$) and tilt and shift matrices.

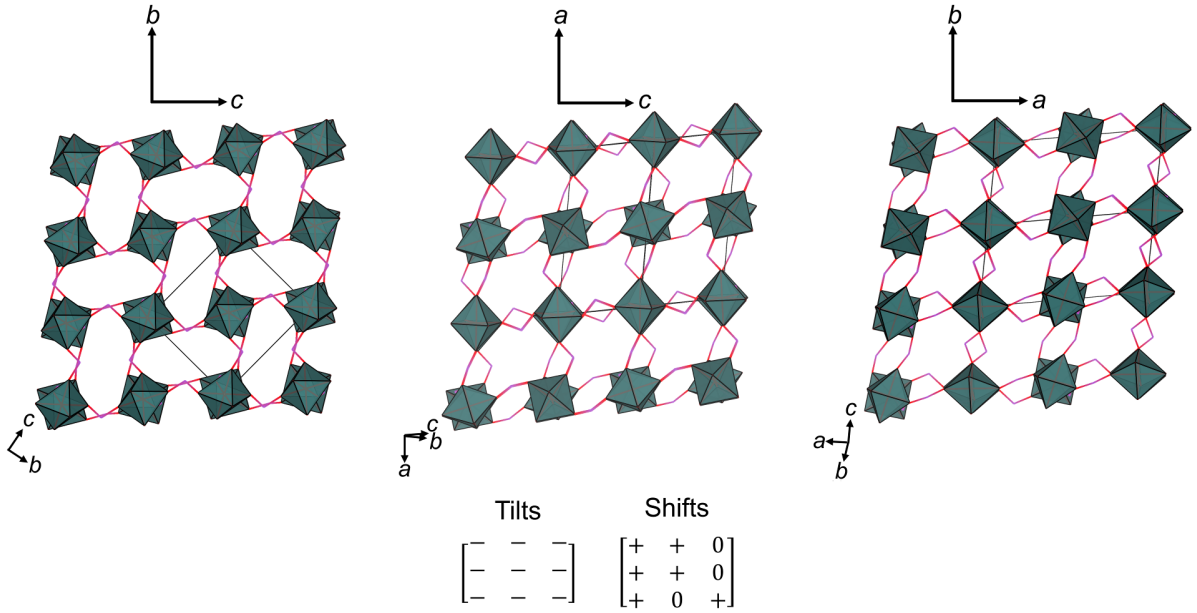

Figure S6: Views of the pseudocubic axes of β-$V(H_2PO_2)_3$ ($P2_1/c$) and tilt and shift matrices.

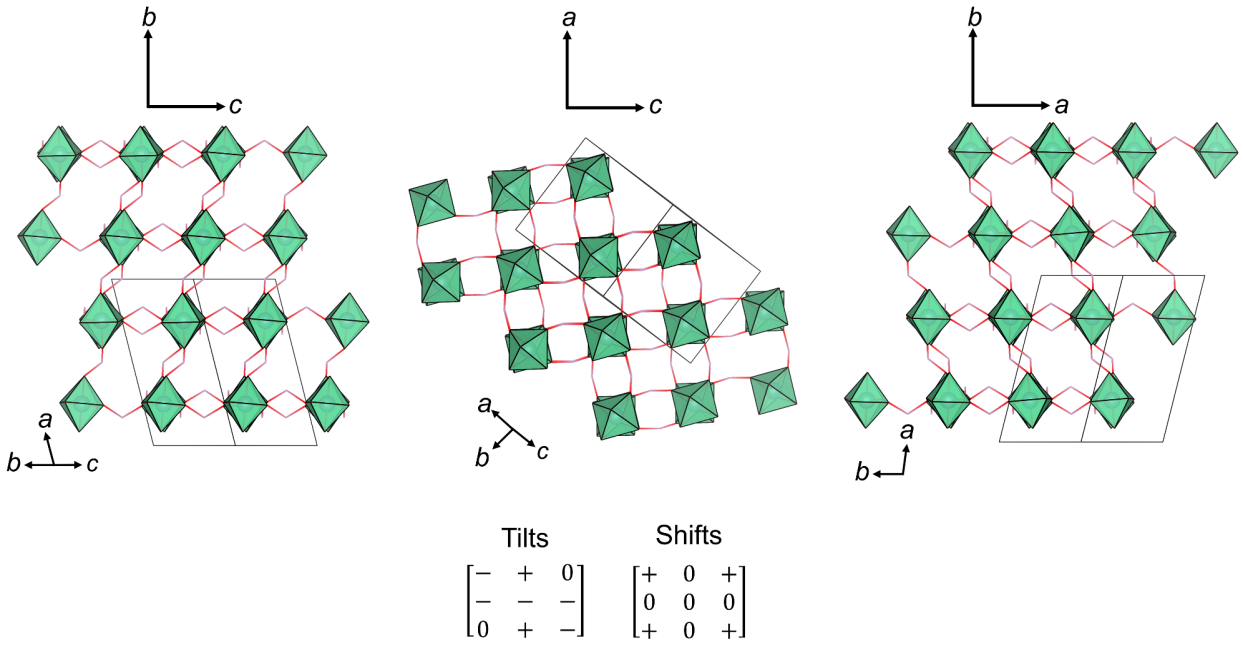

Figure S7: Views of the pseudocubic axes of γ-Al$(H_2PO_2)_3$ ($C2/c$) and tilt and shift matrices.

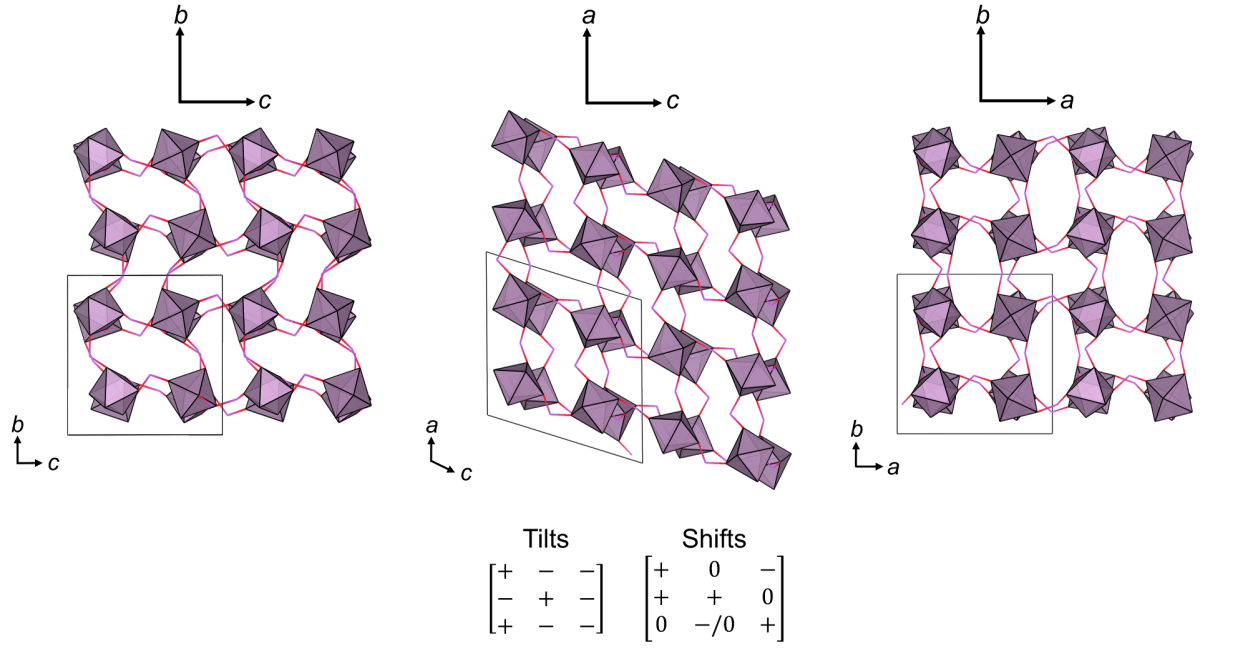

Figure S8: Views of the pseudocubic axes of δ-Ga$(H_2PO_2)_3$ ($P2_1/n$) and tilt and shift matrices. The out-of-phase shift in the psuedocubic b direction in plane c is reduced in magnitude.

Powder X-ray diffraction

Single crystal structural models were used in Rietveld refinements against laboratory PXRD data; these are shown in Figures S9 - S12. Low temperature PXRD data for α-Ga$(H_2PO_2)_3$ compared to room temperature data is shown in Figure S13. The refinements indicate that the each bulk sample has unit cell parameters close to single crystal diffraction dimensions, with the refined lattice parameters listed in Table S3. We were unable to perform high temperature PXRD analysis on the β-V$(H_2PO_2)_3$ and γ-Al$(H_2PO_2)_3$ samples to look for any phase transitions on heating.

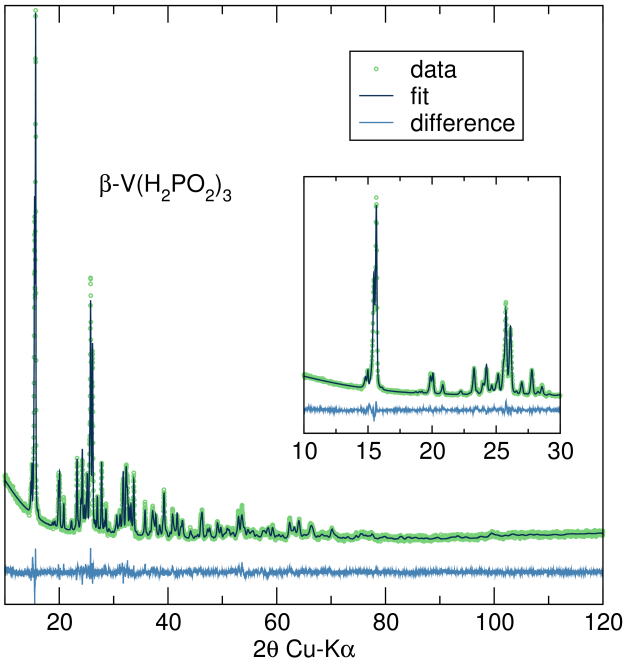

Figure S9: Rietveld refinement of β-V$(H_2PO_2)_3$

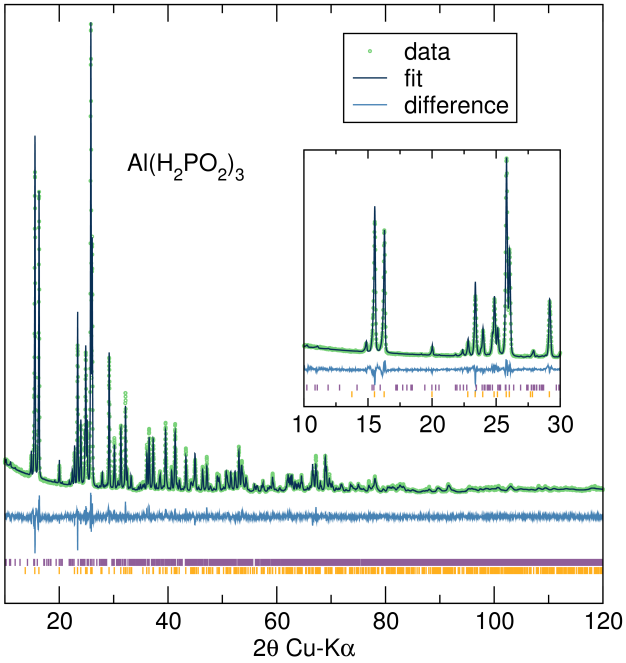

Figure S10: Rietveld refinement of reaction between Al(O-i-Pr)$_3$ and H_3PO_2 which produces both γ-Al$(H_2PO_2)_3$ and α-Al$(H_2PO_2)_3$. Orange ticks = γ, purple ticks = α. The patterns overlap, but indication of a multi-phase product can be noted by the additional peaks near 22 2θ from the α phase. The α phase accounts for ≈10% of the product.

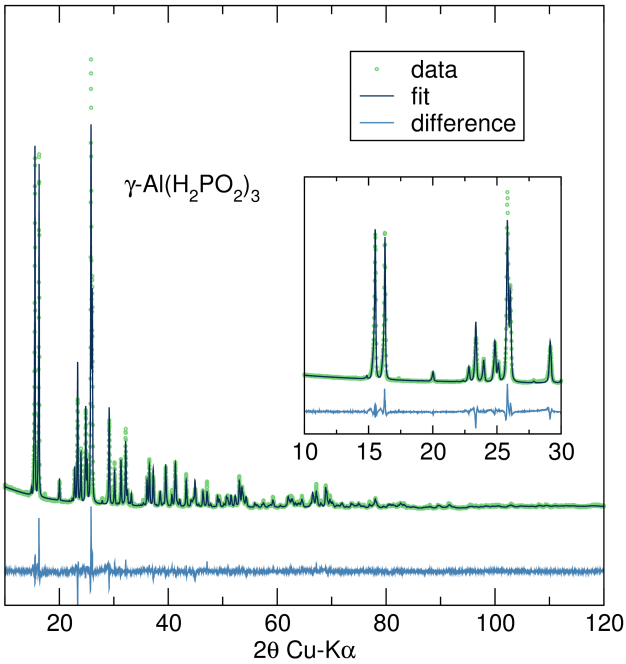

Figure S11: Rietveld refinement of γ-Al$(H_2PO_2)_3$, isolated phase pure by using γ-Al_2O_3 as the Al source.

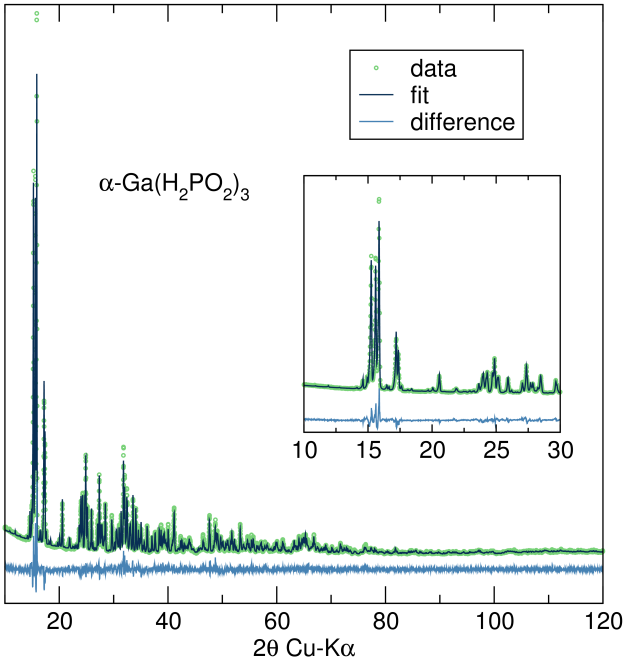

Figure S12: Rietveld refinement of α-Ga$(H_2PO_2)_3$

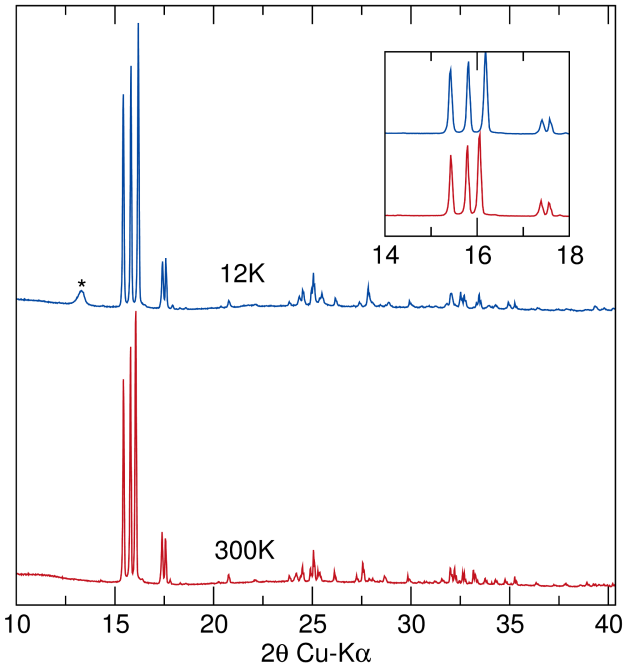

Figure S13: Comparison between 12 K and 300 K powder diffraction data of α-Ga$(H_2PO_2)_3$, illustrating no first order phase transition. The starred peak at 13.5 2θ in the 12 K pattern is an artifact of the low temperature sample stage.

Table S3: Refined lattice parameters of samples that were obtained phase-pure.

Forumla	$V(H_2PO_2)_3$ (β)	$Al(H_2PO_2)_3$ (γ)	$Ga(H_2PO_2)_3$ (α)
a (Å)	11.93	12.25	11.30
b (Å)	7.57	7.80	11.62
c (Å)	8.87	7.97	11.49
α (°)	90	90	90
β (°)	106.32	111.24	98.53
γ (°)	90	90	90

Nuclear magnetic resonance

Figures S14 and S15 show ^{1}H and ^{31}P SPE spectra for α-$Ga(H_2PO_2)_3$, respectively. Only a single major component can be detected in the ^{1}H spectrum centered at 8 ppm. SCXRD indicates 12 distinct hydrogen sites, however strong dipole-dipole couplings between ^{1}H nuclei lead to broad NMR signals which can't be deconvoluted with the resolution available. An apparent minor impurity can be detected at approximately 2 ppm accounting for ≈2% of the overall ^{1}H signal. Again, only a single major component can be seen in the ^{31}P SPE spectrum, centered around 11 ppm. However, the insert depicts structure to the ^{31}P peak.

To improve resolution, ^{1}H decoupling was used to reduce dipolar broadening and obtain a second ^{31}P spectrum, as seen in Figure S16. Here, five components of the ^{31}P spectrum can be simulated using Dmfit software.[28] The parameters of this simulated spectrum can be compared to DFT-GIPAW calculated ^{31}P NMR parameters. Calculated NMR parameters, shown in Table S4, are corrected utilizing a scaling factor and reference shift:[29,30]

$$\delta_{iso} = -k(\sigma_{iso} - \sigma_{ref})$$

Here, the scaling factor, k, was found to be 0.6027 with a reference shift, σ_{ref}, of 299.5 ppm.

Computed isotropic chemical shifts for the relaxed cell structure closely align with the simulated spectrum, allowing for peak assignments. It is apparent from the simulated

spectrum that two ^{31}P sites are represented within the deconvoluted peak centered at 9.0 ppm, corresponding to sites P1 and P3. Calculated chemical shifts for P1 and P3 are separated by less than 1 ppm, leaving their deconvolution beyond the resolution of the spectrum.

For ^{31}P nuclei, T_1 relaxation times are dictated mostly by intramolecular dipolar interactions and can be used to probe reorientational motion, as first described in theory by Bloembergen, Purcell, and Pound.[31] Table S5 shows that the observed ^{31}P sites exhibit no significant difference in measured T_1 times.

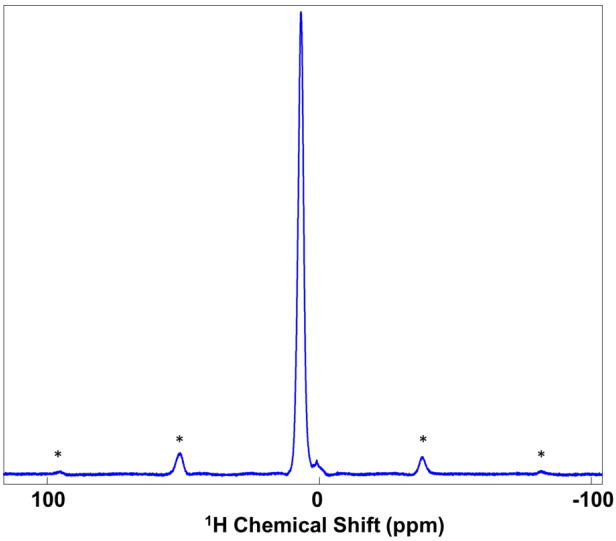

Figure S14: ^{1}H MAS SPE spectrum of α-Ga$(H_2PO_2)_3$. Spinning sidebands are indicated by (*)

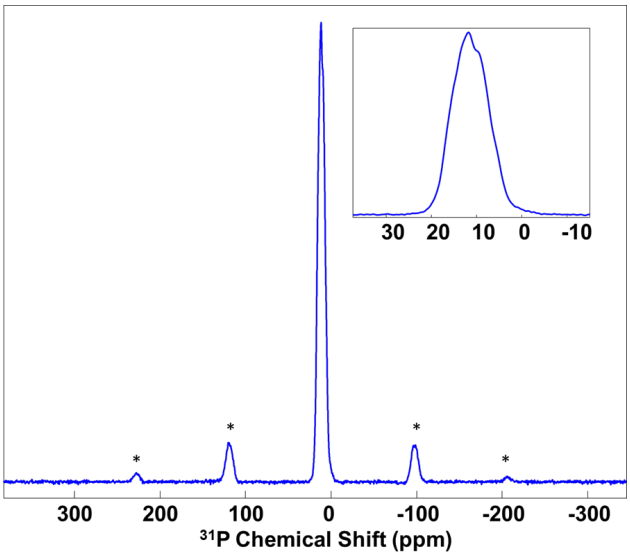

Figure S15: ^{31}P MAS SPE spectrum of α-Ga$(H_2PO_2)_3$. Spinning sidebands indicated by (*)

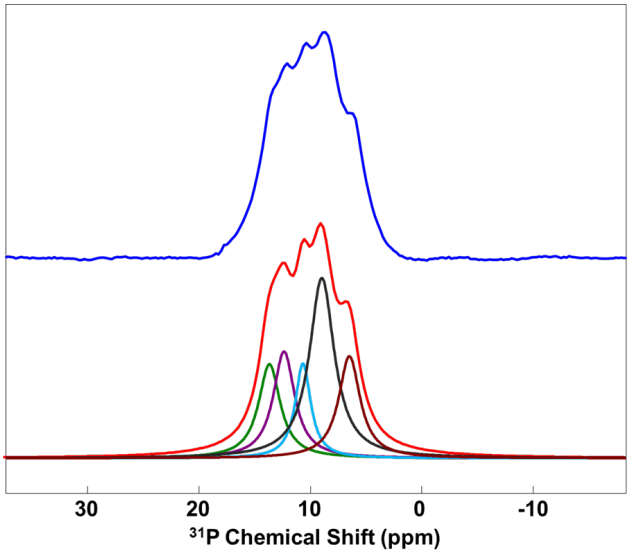

Figure S16: Experimental ^{31}P MAS spectrum with ^{1}H decoupling in blue for α-Ga$(H_2PO_2)_3$. Simulated spectrum below, in red.

Table S4: Comparison of experimental ^{31}P spectrum with GIPAW calculated NMR parameters for α-Ga$(H_2PO_2)_3$.

^{31}P Site	Exp Chem Shift (ppm)	GIPAW Chem Shift (ppm)	GIPAW Corrected (ppm)	Exp Intensity (%)
P4	6.5	-288.1	6.9	18
P1	9.0	-285.7	8.3	36
P3	-	-284.3	9.1	-
P2	10.7	-281.7	10.7	12
P5	12.4	-278.6	12.6	18
P6	13.7	-276.9	13.6	16

Table S5: T_1 relaxation times for five observed ^{31}P sites for α-Ga$(H_2PO_2)_3$.

^{31}P site	T_1 (s)
P1/P3	134 ± 9
P2	136 ± 10
P4	132 ± 9
P5	135 ± 9
P6	135 ± 9

Thermogravimetric analysis (TGA)

Thermogravimetric analysis of the $M(H_2PO_2)_3$ compounds are presented in Figures S17–S18. Both materials show impressive stability, with minimal mass loss up until 900°.

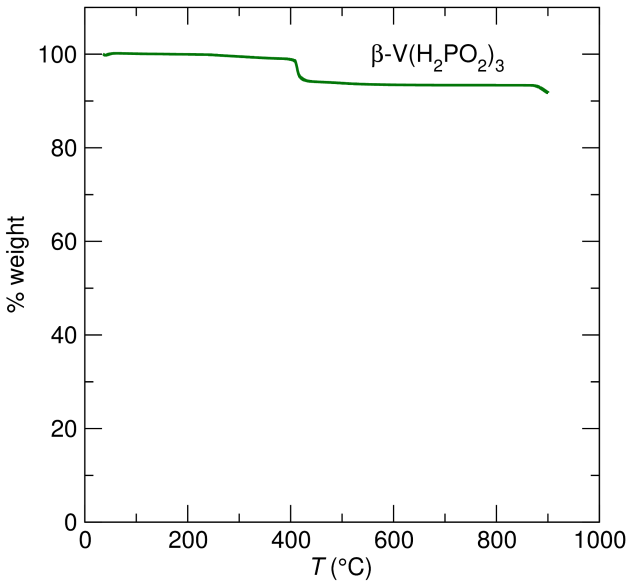

Figure S17: TGA of β-$V(H_2PO_2)_3$ from room temperature to 900°C.

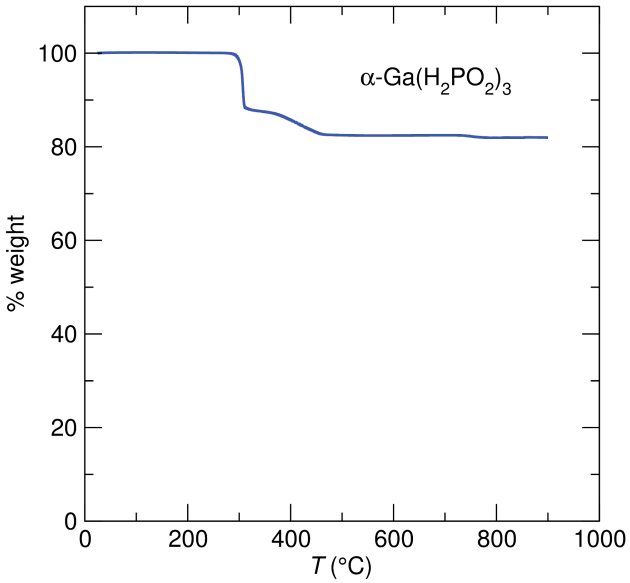

Figure S18: TGA of α-$Ga(H_2PO_2)_3$ from room temperature to 900°C.

Density functional theory calculations

$Ga(H_2PO_2)_3$

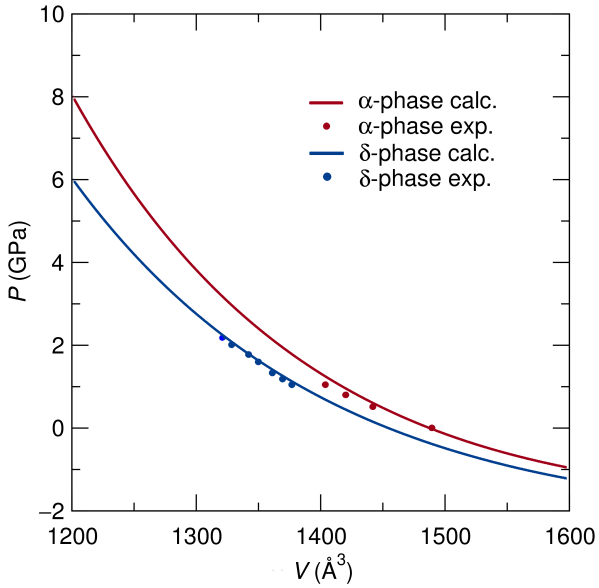

Figure S19: DFT external *P* vs. *V* plots of ambient pressure α-phase and high pressure δ phase for $Ga(H_2PO_2)_3$, as fitted from the Birch-Murnaghan equation of state (details in experimental information section). Points: experimental external *P* vs. *V* plots of α and δ phases.

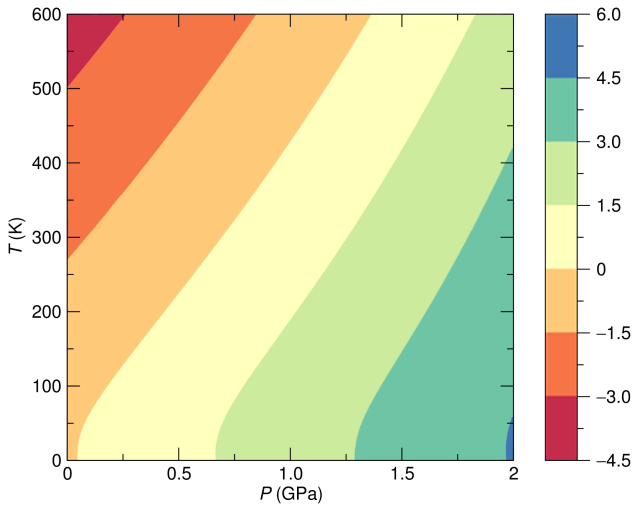

Figure S20: Gibbs free energy difference (α–δ) $Ga(H_2PO_2)_3$ (in kJ/mol *per* f.u.) as a function of *T* and *P*. Noted that there is no phase transition from the α to δ phase when decreasing temperature at 0 *GPa* due to the zero-point vibration.

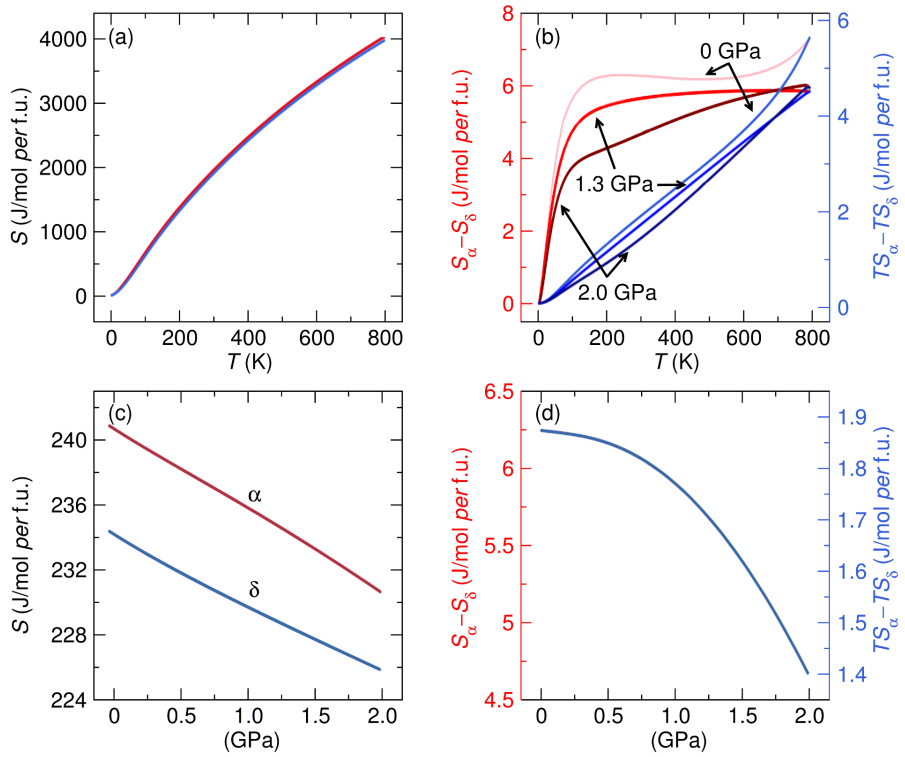

Figure S21: (a) Entropy (S) vs. temperature (T) plot of α (red) and δ (blue) and (b) their differences ($S\alpha$–$S\delta$) at 0 GPa, 1.3 GPa, and 2 GPa. (c) S vs. P plot of α (red) and HP (blue) and (d) their differences at 300 K.

Table S6: Comparison of DFT calculated lattice constants with experimental results for α-$Ga(H_2PO_2)_3$ phase.

	a (Å)	b (Å)	c (Å)	β (°)	V_0 (Å^3)
DFT	11.250	11.635	11.520	98.9	1489.8
Experiment	11.297	11.610	11.486	98.5	1489.9

Table S7: DFT calculated bulk modulus (B) at 300 K for α and β phases.

	α (at 0 GPa)	δ (at 1.3 GPa)
B (GPa)	16.70	24.77

Table S8: Calculated zero-point energy (E_{ZP}) (kJ/mol per f.u.) at ambient pressure for α- and δ-$Ga(H_2PO_2)_3$ phases

	α	δ
E_{ZP}	224.44	225.30

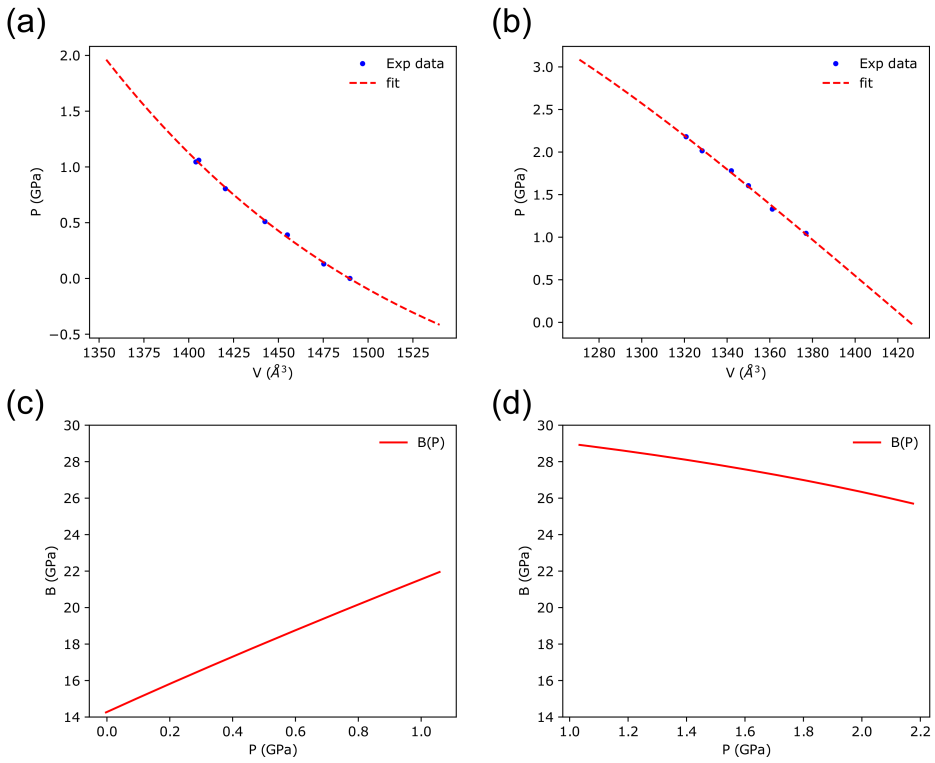

Figure S22: Birch-Murnaghan equation of state fits to experimental data for (a) α-$Ga(H_2PO_2)_3$ and (b) δ-$Ga(H_2PO_2)_3$. Calculated bulk modulus as pressure varies for (c) α-$Ga(H_2PO_2)_3$ and (d) δ-$Ga(H_2PO_2)_3$.

$Al(H_2PO_2)_3$

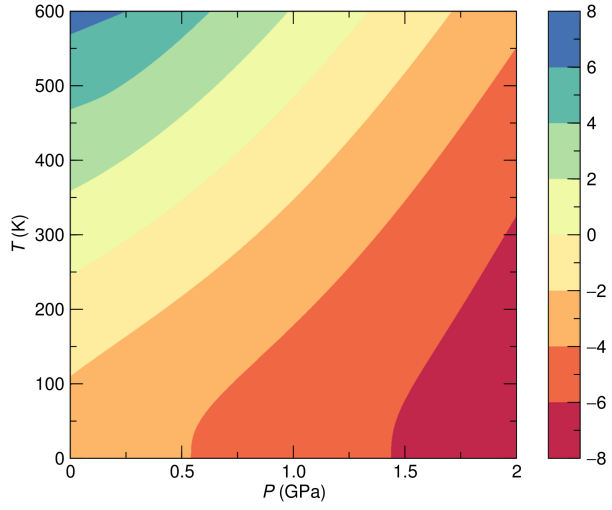

Figure S23: Gibbs free energy difference (α–γ) $Al(H_2PO_2)_3$ (in kJ/mol *per* f.u.) as a function of T and P.

$V(H_2PO_2)_3$

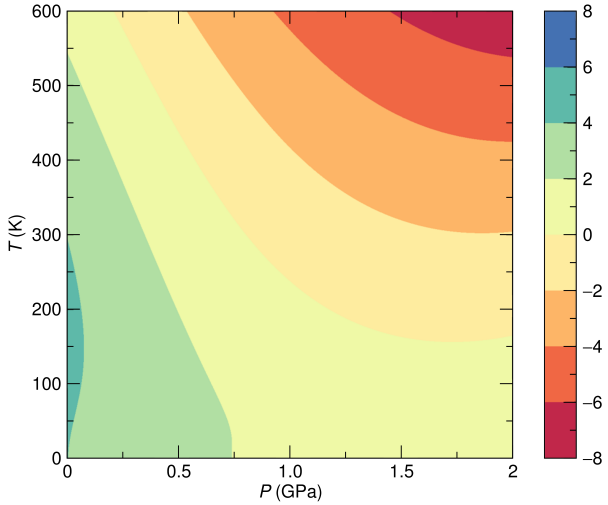

Figure S24: Gibbs free energy difference (α–β) $V(H_2PO_2)_3$ (in kJ/mol *per* f.u.) as a function of *T* and *P*.

References

(1) H. A. Maouel, V. Alonzo, T. Roisnel, H. Rebbah and E. Le Fur, *Acta Cryst. C*, 2009, **65**, i36–i38.

(2) SADABS; G. M. Sheldrich, University of Gottingen: Germany, 2005.

(3) SHELXTL PC, Version 6.12; Bruker AXS Inc.: Madison, WI, 2005.

(4) K. Momma and F. Izumi. *Commission on Crystallogr. Comput.* 2006, **7**, 106–119.

(5) M. Merlini and M. Hanfland, *High Pressure Res.*, 2013, **33**, 511–522.

(6) K. Yokogawa, K. Murata, H. Yoshino and S. Aoyama, *Jpn. J. Appl. Phys., Part 1*, 2007, **46**, 3636–3639.

(7) *Rigaku Oxford Diffraction, (2018), CrysAlisPro Software system, version 1.171.38.46*, Rigaku Corporation, Oxford, UK.

(8) G. M. Sheldrick, *Acta Crystallogr., Sect. C: Struct. Chem.*, 2015, **71**, 3–8.

(9) G. M. Sheldrick, *Acta Crystallogr., Sect. A: Found. Adv.*, 2015, **71**, 3–8.

(10) C. B. Hübschle, G. M. Sheldrick and B. Dittrich, *J. Appl. Crystallogr.*, 2011, **44**, 1281–1284.

(11) C. F. Macrae, P. R. Edgington, P. McCabe, E. Pidcock, G. P. Shields, R. Taylor, M. Towler and J. van de Streek, *J. Appl. Cryst.* 2006, **39**, 453–457.

(12) A. Coelho. *J. Appl. Cryst.* 2018, **51**, 210–218.

(13) P. E. Blöchl, *Phys. Rev. B*, 1994, **50**, 17953–17979.

(14) G. Kresse, *Phys. Rev. B* 1999, **59**, 1758–1775.

(15) G. Kresse and J. Hafner, *Phys. Rev. B*, 1993, **47**, 558–561.

(16) G. Kresse and J. Hafner, *Phys. Rev. B*, 1994, **49**, 14251–14269.

(17) G. Kresse and J. Furthmüller, *Phys. Rev. B*, 1996, **54**, 11169–11186.

(18) G. Kresse and J. Furthmüller, *Comput. Mater. Sci.*, 1996, **6**, 15–50.

(19) H. J. Monkhorst and J. D. Pack, *Phys. Rev. B*, **1976**, *13*, 5188–5192.

(20) J. P. Perdew, K. Burke and M. Ernzerhof, *Phys. Rev. Lett.*, 1997, **77**, 3865–3868.

(21) A. Tkatchenko, M. Scheffler, *Phys. Rev. Lett.* 2009, **102**, 073005.

(22) F. Birch, *Phys. Rev.* 1947, **71**, 809–824.

(23) A. Togo, L. Chaput, I. Tanaka, G. Hug, *Phys. Rev. B* 2010, **81**, 174301.

(24) D. C. Wallace, *Thermodynamics of Crystals*; Courier Corporation, 1998.

(25) C. J. Pickard and F. Mauri, 2001, *Phys. Rev. B* **63**, 245101.

(26) H. L. B. Boström, J. A. Hill, and A. L. Goodwin, *Phys. Chem. Chem. Phys.* 2016, **18**, 31881–31894.

(27) Y. Wu, T. Binford, J. A. Hill, S. Shaker, J. Wang, and A. K. Cheetham, *Chem. Commun.* 2018, **54**, 3751–3754.

(28) D. Massiot, D. 2002, *Magn. Reson. Chem.* **40**, 70–76.

(29) A. Zheng, S. B. Liu, and F. Deng, *J. Phys. Chem. C* 2009, *113*, 15018–15023.

(30) J. M. Griffin, J. R. Yates, A. J. Berry, S. Wimperis, and S. E. Ashbrook, *J. Am. Chem. Soc.* 2010, **132**, 15651–15660.

(31) N. Bloembergen, E M. Purcell, and R. V. Pound, *Phys. Rev.* 1948, **73**, 679–712.